Uncertainty quantification for dynamics of geometrically nonlinear structures coupled with internal acoustic fluids in presence of sloshing and capillarity

Q. Akkaoui[a], E. Capiez-Lernout[a], C. Soize[a,*], R. Ohayon[b]

[a] *Université Paris-Est Marne-la-vallée, Laboratoire Modélisation et Simulation Multi Echelle (MSME) UMR 8208 CNRS, 5 boulevard Descartes, Marne-La-Vallée 77454, France*

[b] *Conservatoire National des Arts et Métiers (CNAM), Structural Mechanics and Coupled Systems Laboratory, 2 rue Conté, Paris 75003, France*

Abstract

In this paper, we propose an uncertainty quantification analysis, which is the continuation of a recent work performed in a deterministic framework. The fluid-structure system under consideration is the one experimentally studied in the sixties by Abramson, Kana, and Lindholm from the Southwest Research Institute under NASA contract. This coupled system is constituted of a linear acoustic liquid contained in an elastic tank that undergoes finite dynamical displacements, inducing geometrical nonlinear effects in the structure. The liquid has a free surface on which sloshing and capillarity effects are taken into account. The problem is expressed in terms of the acoustic pressure field in the fluid, of the displacement field of the elastic structure, and of the normal elevation field of the free surface. The nonlinear reduced-order model constructed in the recent work evoked above is reused for implementing the nonparametric probabilistic approach of uncertainties. The objective of this paper is to present a sensitivity analysis of this coupled fluid-structure system with respect to uncertainties and to use a classical statistical inverse problem for carrying out the experimental identification of the hyperparameter of the stochastic model. The analysis show a significant sensitivity of the displacement of the structure, of the acoustic pressure in the liquid, and of the free-surface elevation to uncertainties in both linear and geometrically nonlinear simulations.

Keywords: Uncertainty quantification, Fluid-structure interactions, Nonlinear dynamics, Reduced-order model, Sloshing, Capillarity

1. Introduction

This paper is the continuation of the work published in (Akkaoui et al., 2019) in order to propose an uncertainty quantification analysis. This previous work consists in a deterministic computational analysis of a linear acoustic liquid contained in an elastic tank that undergoes finite dynamical displacements, inducing geometrical nonlinear effects in the structure (Morand and Ohayon, 1995; Ohayon and Soize, 2016). The fluid-structure system, which has been analyzed, is the one experimentally studied by (Lindholm et al., 1962; Abramson et al., 1966). These experiments have been used for updating the nonlinear dynamical computational model proposed in (Akkaoui et al., 2019) and for analyzing the unexpected phenomenon of very low-frequency sloshing resonance of an internal liquid during a high frequency excitation of the tank. It should be noted that experimental studies for large amplitude vibrations with sloshing liquids have also been performed in the past in other works such as, for instance, in (Abramson et al., 1966; Chiba, 1992; Carra et al., 2013). It should be noted that, in the deterministic context, the case of elastic structure coupling

*Corresponding author
Email address: christian.soize@univ-paris-est.fr (C. Soize)

with liquids with geometric nonlinearities for the structure has been intensively studied using shell theories (see par Amabili (2018)). In this paper, as in the previous paper Akkaoui et al. (2019), we use the general theory of three-dimensional elasticity in finite displacements to model the structure and consequently, its 3D-finite element discretization.

Concerning uncertainty quantification, there are many methodologies and works published, see for instance (Ghanem and Spanos, 1991; Schueller, 2007; Ghanem et al., 2017; Soize, 2017). The objective of this paper is to present a sensitivity analysis of the computational model presented in (Akkaoui et al., 2019) with respect to uncertainties, using the classical nonparametric probabilistic approach of model uncertainties (Soize, 2000, 2017), and is not devoted to the development of novel methodology in uncertainty quantification. It should be noted that the nonparametric probabilistic approach of uncertainties must be implemented on a reduced-order computational model. This is the reason why, the approach proposed in (Mignolet and Soize, 2008; Capiez-Lernout and Soize, 2017) is used for this fluid-structure system. On the other hand, the construction of the reduced-order model can be done using several approaches such as the modal approach, the proper orthogonal decomposition (POD) (Amabili et al., 2003; Amabili and Touzé, 2007; Ballarin and Rozza, 2016), and more advanced approaches such as those reviewed in (Amabili and Paıdoussis, 2003; Mignolet et al., 2013). In this paper, we do not reconsider this question and we reuse the reduced-order model, introduced and validated in (Ohayon and Soize, 2016; Akkaoui et al., 2018, 2019), in order to perform the uncertainty quantification analysis. The reason why an uncertainty quantification of such complex dynamical system has to be carried out is the following: the sensitivity of the unexpected experimental phenomenon, which appears at very low-frequency, has to be quantified in order to analyze the robustness of the sloshing resonances with respect to structural uncertainties.

The paper is organized as follows. Section 2 briefly presents the fluid-structure system that has been experimentally studied by (Lindholm et al., 1962; Abramson et al., 1966), that has been used in (Akkaoui et al., 2019) and that is reused in this paper. The construction of the nonlinear stochastic reduced-order model (SROM) using the nonparametric probabilistic approach is summarized in Section 3 in order to facilitate the reading of this paper. Section 4 is devoted to an uncertainty sensitivity analysis of the dynamical responses of the fluid-structure system with respect to structural uncertainties. Note that the results will be presented for the linearized system and for the nonlinear one. In particular, the sensitivity analysis is carried out for the responses of the structure, of the acoustic liquid, and of the free-surface sloshing. Section 5 deals with the statistical inverse problem that allows for identifying the hyperparameter of structural uncertainties within the context of a given target dataset. In the framework of the uncertainty quantification analysis, since no experimental data were available, we have constructed a dataset of simulated experiments. In the last section, conclusions and discussions are presented.

Notations: In this paper, the following notations are used. Let "a" be a mathematical quantity. Related to such a quantity, a deterministic scalar is denoted by a and its random counterpart by A; a deterministic vector is denoted by $\mathbf{a}$ and its random counterpart by $\mathbf{A}$; a deterministic matrix is denoted by $[A]$ and its random counterpart by $[\mathbf{A}]$. $\mathbb{R}$ denotes the set of real numbers, $\mathbb{R}^p$ denotes the Euclidian space of dimension p, $\mathbb{M}_{m,n}$ denotes the set of real $(m \times n)$ matrices, $\mathbb{M}_n$ denotes the set of real square matrices of size n, $\mathbb{M}_n^+$ denotes the set of positive-definite real square matrices of size n. The summation over repeated Greek and Latin indices is used in the following. For a given function g sufficiently regular, the partial derivative $\partial g(\mathbf{x})/\partial x_j$ is denoted as $g_{,j}(\mathbf{x})$. The first- and second-time derivatives of g are defined by $\dot{g}(\mathbf{x},t) = \partial g(\mathbf{x},t)/\partial t$, and $\ddot{g}(\mathbf{x},t) = \partial^2 g(\mathbf{x},t)/\partial t^2$. The gradient $\nabla_{\mathbf{x}}\,\mathbf{g}(\mathbf{x},t)$ of function $\mathbf{g}$ with respect to $\mathbf{x}$ is defined by $(\nabla_{\mathbf{x}}\,\mathbf{g}(\mathbf{x},t))_{ij} = g_{i,j}$. The Fourier transform of the function $t \mapsto g(\mathbf{x},t)$, with respect to time, is denoted by $\widehat{g}(\mathbf{x},\omega)$ and is defined by

$$\widehat{g}(\mathbf{x},\omega) = \int_{-\infty}^{+\infty} e^{-i\omega t}\, g(\mathbf{x},t)\, dt\,. \tag{1}$$

2. Simulating the experimental results with the nonlinear reduced-order computational model

As explained in Section 1, this section largely reuses the developments presented in (Akkaoui et al., 2019) for which the notations have been adapted.

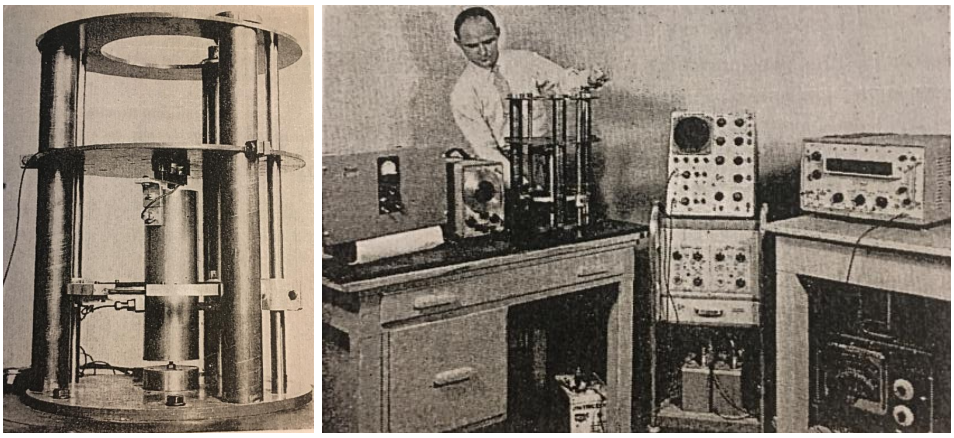

Figure 1: Images of the experimental setup. Figure from (Abramson et al., 1966).

2.1. Finite element modeling of the experimental setup

The fluid-structure system is the one described in (Lindholm et al., 1962; Abramson et al., 1966) for which the retained dimensions are those given in (Abramson et al., 1966). The structure, occupying a bounded domain Ω_u is a steel tank constituted of a thin circular cylinder closed at both ends by circular steel plates. Its isotropic material properties are detailed in (Akkaoui et al., 2019). This tank is partially filled with 30% water. The capillary parameters used for computing the equilibrium position of the free surface (using software Surface Evolver: *www.se-fit.com* (Brakke, 1992)) are the ones given in (Akkaoui et al., 2019) which correspond to classical water-steel contact. The dimensions of the fluid-structure system

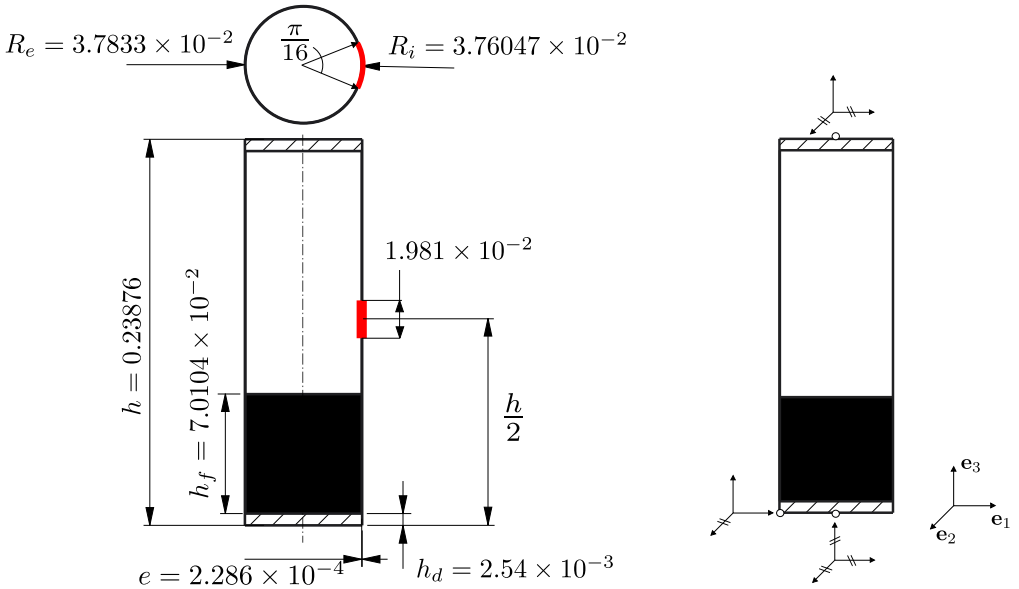

Figure 2: Dimensions of the fluid-structure system (left) and representation of the numerical boundary conditions applied on the system (right). Figure from (Akkaoui et al., 2019).

are given in Figure 2 (left). The origin O of the Cartesian coordinate system $(O, \mathbf{e}_1, \mathbf{e}_2, \mathbf{e}_3)$ is located at the center of the bottom of the cylindrical tank. Axis $\mathbf{e}_3$ coincides with the revolution axis of the system. The numerical boundary conditions applied to the system are the ones displayed in Figure 2 (right). These boundary conditions have been designed in order to match the available experimental data. For more details regarding the computational implementation of the boundary conditions we refer the reader to (Akkaoui et al., 2019). The finite element model of the fluid-structure system displayed in Figure 3 is constructed using 3D tetrahedral quadratic finite elements with 10 nodes for the structure and for the acoustic fluid. The free surface of the liquid is meshed using 2D quadratic finite elements with 6 nodes and the triple line (intersection between the structure and the free surface, which is common to the structure, to the free surface, and to the internal liquid) is meshed using 1D quadratic finite elements with 3 nodes. Table 1 sums up the characteristics of the finite element mesh. In the following, n_p, n_h, and n_u denote respectively the number of degrees of freedom (dof) related to the pressure in the acoustic liquid, to the normal elevation of the free surface, and to the displacement of the elastic structure. The total number of dof of the fluid-structure system is denoted as $n_{phu} = n_p + n_h + n_u$.

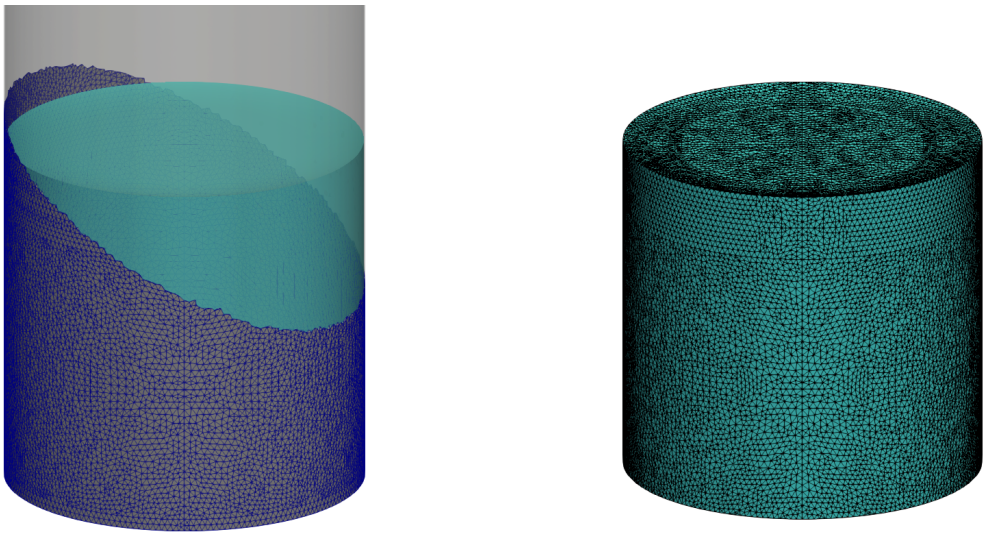

Figure 3: Slice view of the finite element mesh of the structure containing the acoustic liquid (in transparent blue) (left figure). Detailed view of the finite element mesh of the acoustic liquid and of its free surface (right figure).

	Nodes	**Dof**	**Elements**
Fluid	431 354	431 354	296 459
Free surface	11 566	11 566	5 684
Structure	660 385	1 981 155	334 784

Table 1: Table of the finite element mesh properties.

2.2. Nominal nonlinear reduced-order computational model

The nonlinear reduced-order model (ROM), constructed in (Akkaoui et al., 2019), which is used for simulating the experimental setup, is briefly summarized hereinafter. The solution of the coupled problem is expressed in terms of the $\mathbb{R}^{n_p}$-vector $\mathbf{p}$ of the pressure in the internal acoustic liquid, of the $\mathbb{R}^{n_h}$-vector $\mathbf{h}$ of the free-surface normal elevation, and of the $\mathbb{R}^{n_u}$-vector $\mathbf{u}$ of the structural displacement. The construction of this ROM consists in projecting the equations of the fluid-structure system on the reduced-order basis $[\Psi]$ constituted of the vector bases related to each subset of the coupled system described below. The

$(n_{phu} \times N_{phu})$ projection basis $[\Psi]$ is constructed by blocks and is constituted of the $(n_u \times N_u)$ projection basis $[\Phi_u]$ related to the N_u elastic eigenmodes of the structure with added mass effect (simply called the wet elastic modes), of the $(n_p \times N_p)$ projection basis $[\Phi_p]$ related to the N_p acoustic eigenmodes of the internal liquid with zero pressure condition on the free surface for an undeformable structure (simply called the acoustic modes), and of the $((n_p + n_h) \times N_h)$ projection basis $[\Psi_h]$ related to the N_h sloshing-capillarity eigenmodes (simply called the sloshing modes) of the liquid free-surface in presence of the internal liquid for an undeformable structure. The reduced-order basis $[\Psi_h]$ is expressed by blocks as $[\Psi_h] = \left[[\Phi_{ph}]^T [\Phi_h]^T\right]^T$, where $[\Phi_h]$ is the $(n_h \times N_h)$ matrix constituted of the trace of the sloshing modes on the free surface and $[\Phi_{ph}]$ is the $(n_p \times N_h)$ matrix of the pressure in the internal acoustic liquid of these sloshing modes. A time t, the vectors $\mathbf{p}(t)$, $\mathbf{h}(t)$, and $\mathbf{u}(t)$ are written as

$$\begin{bmatrix} \mathbf{p}(t) \\ \mathbf{h}(t) \\ \mathbf{u}(t) \end{bmatrix} = \begin{bmatrix} [\Phi_p] & [\Phi_{ph}] & 0 \\ 0 & [\Phi_h] & 0 \\ 0 & 0 & [\Phi_u] \end{bmatrix} \begin{bmatrix} \mathbf{q}^p(t) \\ \mathbf{q}^h(t) \\ \mathbf{q}^u(t) \end{bmatrix} = [\Psi]\, \mathbf{q}(t)\,, \tag{2}$$

in which $\mathbf{q}(t) = (\mathbf{q}^p(t), \mathbf{q}^h(t), \mathbf{q}^u(t))$ is the $\mathbb{R}^{N_{phu}}$-vector of the generalized coordinates, with $N_{phu} = N_p + N_h + N_u$, which satisfies the following reduced nonlinear differential equation

$$[M_{\mathrm{FSI}}]\, \ddot{\mathbf{q}}(t) + [D_{\mathrm{FSI}}]\, \dot{\mathbf{q}}(t) + [K_{\mathrm{FSI}}]\, \mathbf{q}(t) + \mathbf{f}_{\mathrm{NL}}(\mathbf{q}(t)) = \mathbf{f}(t)\,, \tag{3}$$

in which the $(N_{phu} \times N_{phu})$ matrices $[M_{\mathrm{FSI}}]$, $[D_{\mathrm{FSI}}]$, $[K_{\mathrm{FSI}}]$, and the $\mathbb{R}^{N_{phu}}$ vector $\mathbf{f}(t)$ are defined as

$$[M_{\mathrm{FSI}}] = [\Psi]^T \begin{bmatrix} [M] & -[C_{ph}]^T & -[C_{pu}]^T \\ 0 & 0 & 0 \\ 0 & 0 & [M_u] \end{bmatrix} [\Psi]\,, \tag{4}$$

$$[D_{\mathrm{FSI}}] = [\Psi]^T \begin{bmatrix} [D] & 0 & 0 \\ 0 & 0 & 0 \\ 0 & 0 & [D_u] \end{bmatrix} [\Psi]\,, \tag{5}$$

$$[K_{\mathrm{FSI}}] = [\Psi]^T \begin{bmatrix} [K] & 0 & 0 \\ [C_{ph}] & [K_{gc}] & [C_{hu}] \\ [C_{pu}] & [C_{hu}]^T & [K_u] \end{bmatrix} [\Psi]\,, \tag{6}$$

$$\mathbf{f}(t) = [\Psi]^T \begin{bmatrix} 0 \\ 0 \\ \mathbf{f}_u(t) \end{bmatrix}\,. \tag{7}$$

In Eq. (3), $\mathbf{f}_{\mathrm{NL}}(\mathbf{q})$ denotes the nonlinear conservative contribution of the geometrical nonlinearities of the structure that is computationally directly constructed in the reduced form without explicitly assembling the finite elements (see (Mignolet and Soize, 2008; Capiez-Lernout et al., 2012)). The generalized conservative internal nonlinear forces are written as

$$f_{\mathrm{NL}}(\mathbf{q})_\alpha = K^{(2)}_{\alpha\beta\gamma}\, q^u_\beta\, q^u_\gamma + K^{(3)}_{\alpha\beta\gamma\delta}\, q^u_\beta\, q^u_\gamma\, q^u_\delta\,, \tag{8}$$

where the quadratic and cubic stiffnesses $K^{(2)}_{\alpha\beta\gamma}$ and $K^{(3)}_{\alpha\beta\gamma\delta}$ are such that

$$K^{(2)}_{\alpha\beta\gamma} = \frac{1}{2}\left(\widehat{K}^{(2)}_{\alpha\beta\gamma} + \widehat{K}^{(2)}_{\beta\gamma\alpha} + \widehat{K}^{(2)}_{\gamma\alpha\beta}\right)\,, \tag{9}$$

$$\widehat{K}^{(2)}_{\alpha\beta\gamma} = \int_{\Omega_u} C_{ijk\ell}\, \varphi^\alpha_{i,j}\, \varphi^\beta_{m,k}\, \varphi^\gamma_{m,\ell}\, d\mathbf{x}\,, \tag{10}$$

$$K^{(3)}_{\alpha\beta\gamma\delta} = \frac{1}{2}\int_{\Omega_u} C_{ijk\ell}\, \varphi^\alpha_{s,i}\, \varphi^\beta_{s,j}\, \varphi^\gamma_{m,k}\, \varphi^\delta_{m,\ell}\, d\mathbf{x}\,, \tag{11}$$

in which C denotes the fourth-order elasticity tensor.

2.3. Validation of the computational model and eigenfrequency characterization

The validation of the computational model of the experimental setup has been carried out by comparing the experimental and the computational eigenfrequencies of the structure *in vacuo*, that is to say, the eigenfrequencies of the dry elastic modes (Akkaoui et al., 2019). On the other hand, the eigenfrequency characterization of the fluid-structure system is summarized in Figure 4. One can see that the first wet elastic mode has an eigenfrequency $\nu_1^u = 657\,Hz$ and that the first acoustic mode has an eigenfrequency $\nu_1^p = 5\,194\,Hz$. Note that the modal density of the sloshing modes is important since $\nu_{500}^h = 57.78\,Hz$. It should be noted that, in the reduced-order model, all the wet elastic modes (see the meaning at the

Frequency	0	500	2 500	6 000	12 500
Acoustic				$\nu_1^p = 5\,194$	
Sloshing	$\nu_1^h = 3.44$ $\nu_{500}^h = 57.78$				
Elastic		$\nu_1^s = 657$	$\nu_{31}^s = 2\,482$	$\nu_{141}^s = 5\,934$	

Figure 4: Table of the eigenfrequency characterization (in Hz) of the fluid-structure system: eigenfrequencies of acoustic modes, sloshing modes, and wet elastic modes.

beginning of Section 2.2) have been taken into account in the frequency band for this axisymmetric system: the wet elastic modes having a circumferential wave number $n = 0$ and all the wet elastic modes having a circumferential wave number $n \geq 1$. It should be noted that the rank of the first $n = 0$ dry elastic mode (without the added mass effect) is 89 and its associated eigenfrequency is $4\,509\,Hz$. The rank of the corresponding wet elastic mode is 32 and its associated eigenfrequency is $1\,852\,Hz$ (important shift due to the added mass). The convergence analysis that was performed has shown that the optimal values of the reduced-order model is obtained fo $N_u = 60$, $N_p = 40$, and $N_h = 1,500$.

2.4. Dynamical excitation for the deterministic simulations

The dynamical excitation of the system is a time-dependent force chosen such that its Fourier transform is a constant in the frequency band of excitation $\mathbb{B}_e = [\nu_{min}\,,\,\nu_{max}]\,Hz$ with $\nu_{min} = 500\,Hz$ and $\nu_{max} = 2\,500\,Hz$ in order to excite only the wet elastic modes. There are sloshing modes in the frequency band of excitation $\mathbb{B}_e$ but their contributions in this band are negligible. Only the sloshing modes whose eigenfrequencies are below $500\,Hz$ are kept for constructing the ROM. It can be seen that the first $n = 0$ elastic mode ($\nu^u = 1\,852\,Hz$) belongs to the frequency band of excitation. There is no other $n = 0$ wet elastic eigenmode whose rank is less than or equal to 100. The time-dependent external load vector $\mathbf{f}_u(t)$ (see Eqs. (3) and (7)) is written as

$$\mathbf{f}_u(t) = \alpha\, g(t)\, \mathbb{F}\,, \tag{12}$$

in which α is the intensity coefficient taken as $\alpha = 4$, $g(t)$ is the time function of the dynamical excitation, and $\mathbb{F}$ is the normalized vector representing the spatial distribution of the external time load. The excitation is radially oriented and located on a small rectangular patch (see the red patch in Figure 2 (left)). In Eq. (12), the time signal $g(t)$ is chosen such that its Fourier transform $\widehat{g}(2\pi\nu)$ is written as

$$\widehat{g}(2\pi\nu) = 1 \text{ for } \nu \in \mathbb{B}_e \cup \underline{\mathbb{B}}_e \text{ and } = 0 \text{ otherwise}\,, \tag{13}$$

in which $\underline{\mathbb{B}}_e = [-\nu_{max}\,,\,-\nu_{min}]$. The computation is carried out the time domain $[t_{ini},\, t_{ini} + T]$ such that $t_{ini} = -1.28\,s$ and $T = 21\,s$. The sampling frequency and the number of time steps are chosen as $\nu_e = 25\,000\,Hz$ and $N_t = 524\,288$. The frequency response of the system in the band $\mathbb{B}_a = [0,\, 6\,000]\,Hz$ is deduced by a Fourier transform.

2.5. Recall of the explanation concerning the unexpected sloshing phenomenon at very low frequency

The numerical results presented in (Akkaoui et al., 2019) have allowed for concluding that the high-amplitude motion of the free surface in the very low frequency band (outside the frequency band of excitation) could be explained by the couplings illustrated in Figure 5 and recalled hereinafter. The geometrical nonlinearities of the structure induce a transfer of the vibrational energy from the high-frequency band of excitation in the very low- and low-frequency band (outside the frequency band of excitation). As the first acoustic modes of the liquid is greater than the upper bound of the high-frequency band of excitation, the acoustic fluid has a quasistatic behavior in the low-frequency band. Therefore, the energy transferred by the structure in the very low-frequency band is transmitted through the acoustic liquid to the first very low-frequency sloshing modes. This means that the observed phenomenon appears to be an *indirect* transfer of energy from the structure to the free surface through the acoustic liquid, due to the geometrical nonlinearities of the elastic tank.

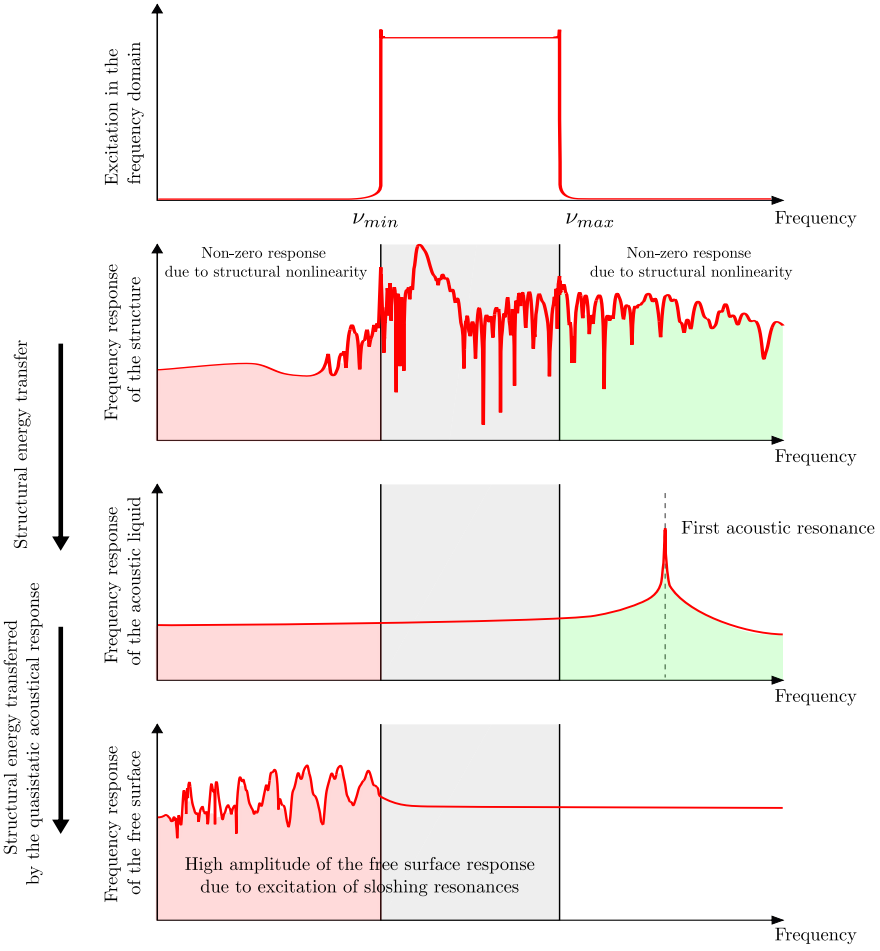

Figure 5: Scheme of the energy transfers between the nonlinear structure, the linear acoustic liquid, and the linear free surface, which explain the excitation of the first sloshing modes in the very low frequency band (outside the frequency band of the external excitations).Figure from (Akkaoui et al., 2019).

3. Nonparametric stochastic model of uncertainties in the nonlinear dynamical computational model

The main source of uncertainty is due to the elastic structure for which geometrical nonlinearities are taken into account. For such a slender and thin-wall structure, the model uncertainties on the stiffness can be significant. Especially when geometrical nonlinearities are taken into account due to the sensitivity of the quadratic and cubic terms in the nonlinear restoring forces. This is why, in the following, we are interested in constructing a stochastic reduced-order model (SROM) in which the linear and nonlinear stiffness forces are uncertain and for which the nonparametric probabilistic approach is used according to the explanation given in Section 1.

3.1. Nonparametric stochastic computational model

In this section, we extend the construction of the SROM proposed in (Mignolet and Soize, 2008; Capiez-Lernout and Soize, 2017) for a structure, to the case of the fluid-structure system considered in this paper. The stochastic nonlinear reduced-order computational model is constructed using the ROM and is written as

$$\begin{bmatrix} \mathbf{P}(t) \\ \mathbf{H}(t) \\ \mathbf{U}(t) \end{bmatrix} = \begin{bmatrix} [\Phi_p] & [\Phi_{ph}] & 0 \\ 0 & [\Phi_h] & 0 \\ 0 & 0 & [\Phi_u] \end{bmatrix} \begin{bmatrix} \mathbf{Q}^p(t) \\ \mathbf{Q}^h(t) \\ \mathbf{Q}^u(t) \end{bmatrix} = [\Psi]\, \mathbf{Q}(t)\,, \tag{14}$$

in which, for all time t, the random vector $\mathbf{Q}(t)$ satisfies the following stochastic nonlinear differential equation

$$[M_{\mathrm{FSI}}]\, \ddot{\mathbf{Q}}(t) + [D_{\mathrm{FSI}}]\, \dot{\mathbf{Q}}(t) + [\mathbf{K}_{\mathrm{FSI}}]\, \mathbf{Q}(t) + \mathbf{F}_{\mathrm{NL}}(\mathbf{Q}(t)) = \mathbf{f}(t)\,. \tag{15}$$

In Eq. (15) $[\mathbf{K}_{\mathrm{FSI}}]$ and $\mathbf{F}_{\mathrm{NL}}(\mathbf{Q})$ denote respectively the $(N_{phu} \times N_{phu})$ random linear stiffness matrix and the $\mathbb{R}^{N_{phu}}$ random vector of nonlinear restoring forces. The random linear fluid-structure stiffness matrix $[\mathbf{K}_{\mathrm{FSI}}]$ can be expressed by blocks as

$$[\mathbf{K}_{\mathrm{FSI}}] = \begin{bmatrix} [K_{11}] & [K_{12}] & [0] \\ [K_{21}] & [K_{22}] & [K_{23}] \\ [K_{31}] & [K_{32}] & [\mathbf{K}_{33}] \end{bmatrix}\,, \tag{16}$$

in which $[\mathbf{K}_{33}]$ is the random counterpart of matrix $[K_{33}]$, which belongs to the set $\mathrm{SE}^+_\varepsilon$ defined in Appendix A. The random vector $\mathbf{F}_{\mathrm{NL}}$ is expressed as a function of the random quadratic and cubic stiffness tensors, $\mathbf{K}^{(2)}$ and $\mathbf{K}^{(3)}$, such that

$$\{\mathbf{F}_{\mathrm{NL}}(\mathbf{q})\}_\alpha = \mathbf{K}^{(2)}_{\alpha\beta\gamma}\, q^u_\beta\, q^u_\gamma + \mathbf{K}^{(3)}_{\alpha\beta\gamma\delta}\, q^u_\beta\, q^u_\gamma\, q^u_\delta\,. \tag{17}$$

The random variables $[\mathbf{K}_{33}]$, $\mathbf{K}^{(2)}$, and $\mathbf{K}^{(3)}$ are statistically dependent. The construction of these random variables is detailed in (Mignolet and Soize, 2008) and is summarized below. Let us introduce the following deterministic $(N_K \times N_K)$ matrix, with $N_K = N_u(1 + N_u)$,

$$[K] = \begin{bmatrix} [K_{33}] & [\widehat{K}^{(2)}] \\ [\widehat{K}^{(2)}]^T & 2[K^{(3)}] \end{bmatrix}\,, \tag{18}$$

in which $[\widehat{K}^{(2)}]$ and $[K^{(3)}]$ denote respectively the matrices issued from the following reshaping:

$$[\widehat{K}^{(2)}]_{\alpha B} = \widehat{K}^{(2)}_{\alpha\beta\gamma}, \quad \text{with} \quad B = (\beta - 1)N_u + \gamma\,, \tag{19}$$

$$[K^{(3)}]_{AB} = K^{(3)}_{\alpha\beta\gamma\delta}, \ \text{with}\ A = (\alpha - 1)N_u + \beta \ \text{ and } \ B = (\gamma - 1)N_u + \delta\,. \tag{20}$$

It is shown in (Mignolet and Soize, 2008) that matrix $[K]$ is positive definite and can consequently be written as $[K] = [L_K]^T\, [L_K]$. Thus, the nonparametric probabilistic approach can be applied in the geometrically nonlinear context on matrix $[K]$, which ensures the statistical dependency of each linear and nonlinear stiffness matrices. The construction of the random matrix $[\mathbf{K}]$, which is the random counterpart of $[K]$, is

chosen in ensemble $\mathrm{SE}_\varepsilon^+$. However, from a numerical point of view, $\mathrm{SE}_\varepsilon^+ \sim \mathrm{SE}_0^+$ for $\varepsilon = 10^{-6}$. In order to simplify the following algebraic developments, we choose $[\mathbf{K}]$ in SE_0^+,

$$[\mathbf{K}] = [L_K]^T \, [\mathbf{G}_0(\delta)] \, [L_K] \, , \tag{21}$$

in which the random matrix germ $[\mathbf{G}_0(\delta)]$ belongs in the ensemble SG_0^+, defined in Appendix A. The expressions of random variables $[\mathbf{K}_{33}]$, $\widehat{\mathbf{K}}^{(2)}$, and $\mathbf{K}^{(3)}$ are deduced from an extraction of $[\mathbf{K}]$. The random variable $\mathbf{K}^{(2)}$ is then reconstructed from $\widehat{\mathbf{K}}^{(2)}$ similarly to Eq. (9). However, it has been shown in (Capiez-Lernout and Soize, 2017) that some difficulties can be encountered with this construction, due to the dimension $(N_K \times N_K)$ of random matrix $[\mathbf{K}]$, for which the number of entries is $N_u^2(1+N_u)^2 \sim N_u^4$ that can be very large (for $N_u = 60$, there are $12,960,000$ random variables). Such a large number of random variables is not necessary for the probabilistic model and penalizes the computational cost. The modification of the stochastic model for $[\mathbf{K}]$, proposed in (Capiez-Lernout and Soize, 2017) is used. This formulation uses another factorization of matrix $[K]$ by introducing a matrix of size $(\widetilde{N}_K \times N_K)$ with $\widetilde{N}_K \ll N_K$ based on the following eigenvalue problem

$$[K] \, [\Phi_K] = [\Phi_K] \, [\Lambda_K] \quad , \quad [\Phi_K]^T \, [\Phi_K] = [I_{N_K}] \, , \tag{22}$$

in which the entries of the diagonal matrix $[\Lambda_K]$ are the eigenvalues λ_α, and where the associated columns of $[\Phi_K]$ are the eigenvectors $\boldsymbol{\varphi}_K^\alpha$. Matrix $[K]$ can then be approximated by the $(N_K \times N_K)$ matrix $[\widetilde{K}]$ such that

$$[\widetilde{K}] = [\widetilde{L}]^T \, [\widetilde{L}] \, , \tag{23}$$

in which $[\widetilde{L}]$ is the full $(\widetilde{N}_K \times N_K)$ matrix defined by

$$[\widetilde{L}] = [\Lambda_K^{\widetilde{N}_K}]^{\frac{1}{2}} \, [\Phi_K^{\widetilde{N}_K}]^T \, , \tag{24}$$

where $[\Lambda_K^{\widetilde{N}_K}]$ is the $(\widetilde{N}_K \times \widetilde{N}_K)$ diagonal eigenvalue matrix such that $[\Lambda_K^{\widetilde{N}_K}]_{\alpha\alpha} = \lambda_\alpha$ sorted by decreasing order $(\lambda_1 \geq \lambda_2 \geq \ldots \geq \lambda_{\widetilde{N}_K})$, and where $[\Phi_K^{\widetilde{N}_K}]$ is the matrix containing the $\widetilde{N}_K$ eigenvectors $\{\boldsymbol{\varphi}_K^\alpha\}_{\alpha=1,\ldots,\widetilde{N}_K}$ associated with eigenvalues λ_α. In order to find the optimal value of $\widetilde{N}_K$, the error fuction $\widetilde{N}_K \mapsto \mathrm{Conv}_K(\widetilde{N}_K)$is introduced such that

$$\mathrm{Conv}_K(\widetilde{N}_K) = \sqrt{\frac{\| \, [\widetilde{K}] - [K] \, \|_F^2}{\| \, [K] \, \|_F^2}} \tag{25}$$

in which $|| \, [K] \, ||_F$ denotes the Frobenius norm of matrix $[K]$. The order $\widetilde{N}_K$ of the truncature is determined for a given relative error ε_K such that $\mathrm{Conv}_K(\widetilde{N}_K) \leq \varepsilon_K$. The random matrix $[\mathbf{K}]$ is then replaced by the random matrix $[\widetilde{\mathbf{K}}]$ such that

$$[\widetilde{\mathbf{K}}] = [\widetilde{L}]^T \, [\widetilde{\mathbf{G}}_0(\delta)] \, [\widetilde{L}] + ([K] - [\widetilde{K}]) \, . \tag{26}$$

in which $[\widetilde{\mathbf{G}}_0(\delta)]$ is the $(\widetilde{N}_K \times \widetilde{N}_K)$ random matrix that belongs to SG_0^+. It should be noted that Eq. (26) ensures that matrix $[\widetilde{\mathbf{K}}]$ is almost surely positive-definite and, in addition, for $\delta = 0$, $[\widetilde{\mathbf{K}}] = [K]$.

3.2. Observations and quantities of interest

The dynamical response of the fluid-structure system is analyzed for different observation nodes of the finite element mesh. These observations nodes, and their associated coordinates are given in Table 2. A node, denoted $\mathbf{x}^p$, is chosen for the observation of the pressure in the acoustic liquid. A node, common to both the structure and the free surface is chosen on the triple line. This common node is denoted $\mathbf{x}_1^h$ for observing the normal elevation of the free surface and is denoted $\mathbf{x}^u$ for observing the structural displacement. Finally, a sloshing observation node $\mathbf{x}_2^h$ is chosen at the center of the free surface. The quantities of interest are therefore explicited at these observation nodes. In order to quantify the influence of the geometrical nonlinearities on the uncertainty propagation in the fluid-structure system, *linear computations* (*i.e.* considering $\mathbf{F}_{\mathrm{NL}}(\mathbf{Q}(t)) = \mathbf{0}$) and *nonlinear computations* are performed. In the following, the superscripts L and NL denote respectively the quantities calculated for the linear case and for the nonlinear case.

Location	Name	x_1-coordinate	x_2-coordinate	x_3-coordinate
Liquid	$\mathbf{x}^p$	0.0187	0	0.0076
Free surface	$\mathbf{x}_1^h$	-0.0144	-0.0347	0.1248
	$\mathbf{x}_2^h$	0	0	0.1245
Structure	$\mathbf{x}^u$	-0.0144	-0.0347	0.1248

Table 2: Coordinates of the observation nodes for the fluid, the free surface, and the structure.

- For the structural displacement, the quantity of interest dB^U, calculated with both the linear and the nonlinear SROM, is defined as the displacement at the node $\mathbf{x}^u$ (see Table 2 for its coordinates) and is written as

$$dB^{U^{\mathrm{L/NL}}} = 20\log_{10}\left(\|\widehat{\mathbf{U}}_{\mathbf{x}^u}^{\mathrm{L/NL}}(2\pi\nu)\|_{\mathbb{C}^3}\right) . \tag{27}$$

- For the pressure in the acoustic liquid, the quantity of interest dB^P, calculated with both the linear and the nonlinear SROM, is defined as the pressure at the observation node $\mathbf{x}^p$ (see Table 2 for its coordinates) and written as

$$dB^{P^{\mathrm{L/NL}}}(2\pi\nu) = 20\log_{10}(\,|\widehat{P}_{\mathbf{x}^p}^{\mathrm{L/NL}}(2\pi\nu)|\,) \quad , \tag{28}$$

- For the free surface elevation, the quantity of interest dB^H, calculated with both the linear and the nonlinear SROM, is defined as the normal elevation at the observation nodes $\mathbf{x}_k^h$, $k = 1, 2$ (see Table 2 for their coordinates) and written as

$$dB_k^{H^{\mathrm{L/NL}}}(2\pi\nu) = 20\log_{10}(\,|\widehat{H}_{\mathbf{x}_k^h}^{\mathrm{L/NL}},(2\pi\nu)|\,) \quad , \tag{29}$$

For each quantity of interest, a confidence region with 95% confidence is estimated using a stochastic solver based on the Monte-Carlo numerical method for generating the N_r realizations of the nonlinear random responses.

4. Uncertainty sensitivity analysis on the dynamical responses of the fluid-structure system

The uncertainty sensitivity of the model is analyzed for each part of the system, namely the structure, the internal liquid, and the free surface. In the following sections, we are interested in quantifying the influence of the hyperparameter δ (controlling the level of uncertainties) on the 95% confidence region of the dynamical responses at the observation nodes. A convergence analysis with respect to N_r is performed in order to ensure the convergence of the confidence region computed for each quantity of interest. This convergence analysis yields an optimal value $N_r = 256$ of Monte Carlo realizations. The results are presented for both the linear and nonlinear stochastic ROM. The nominal dynamical response of the quantity of interest, which corresponds to the deterministic computation of the fluid-structure system, is superimposed with the confidence region of the stochastic responses.

4.1. Sensitivity of the structural responses to uncertainties

The sensitivity of the structural responses to uncertainties is shown in Figure 6, which displays the linear and the nonlinear nominal frequency responses $dB^{U^{\mathrm{L}}}$ and $dB^{U^{\mathrm{NL}}}$, and the associated confidence region, for three values of hyperparameter $\delta \in \{0.05, 0.15, 0.30\}$. It can be seen that uncertainty tends to spread in the low- and high- frequency domains due to energy transfer induced by the geometrical nonlinearities of the structure. The results show a significant, if not a great, sensitivity of the displacements of the structure to structural uncertainties.

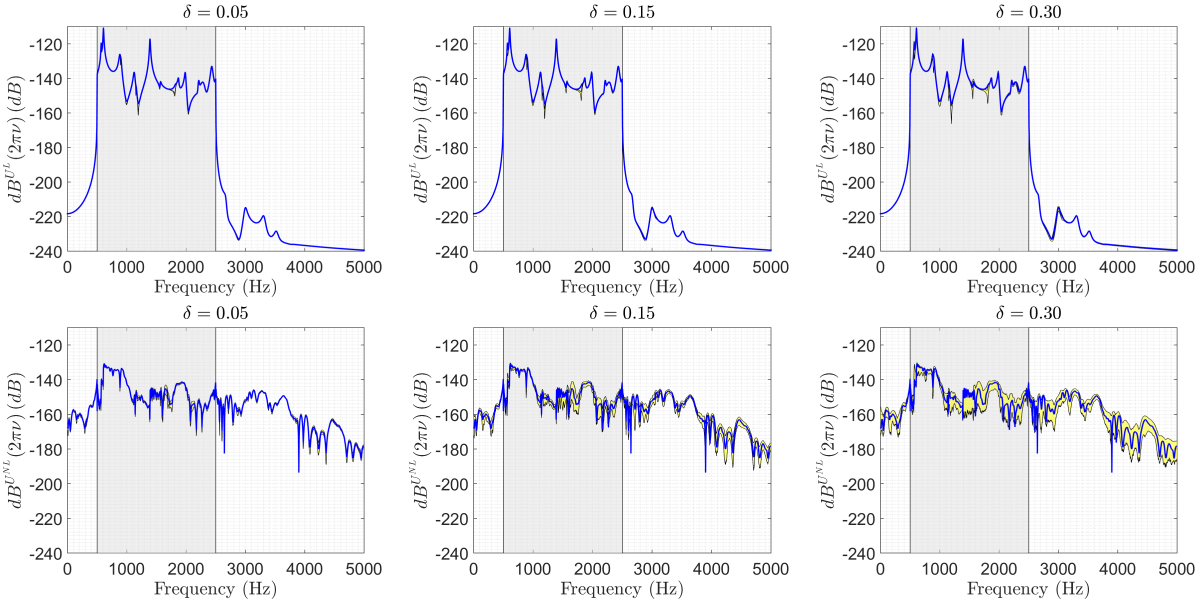

Figure 6: Nominal dynamical responses and confidence regions at 95% of the linear (top figures) and nonlinear (bottom figures) structural displacement at the observation point $\mathbf{x}^u$ for $\delta = 0.05$ (left), for $\delta = 0.15$ (middle), and for $\delta = 0.30$ (right).

4.2. Sensitivity of the acoustic liquid to structural uncertainties

The sensitivity of the acoustic liquid to structural uncertainties is presented in Figure 7. It can be seen that the uncertainty propagation in the acoustic liquid is very important both in the linear and in the nonlinear cases. The results of the linear simulations show that the width of the confidence region is significant for a low dispersion rate $\delta = 0.05$. In addition, it can be seen that the nominal dynamic response of the system in the excitation band $\mathbb{B}_e$ tends to exit this confidence region when δ increases. The same phenomenon is visible for nonlinear responses.

4.3. Sensitivity of the free-surface sloshing to structural uncertainties

The sensitivity of the free-surface sloshing to structural uncertainties is presented in Figures 8 and 9 for the observation nodes $\mathbf{x}_1^h$ and $\mathbf{x}_2^h$. The first observation node $\mathbf{x}_1^h$, located on the triple line, is less sensitive to uncertainties (both in the linear and in the nonlinear cases) than the node $\mathbf{x}_2^h$ located at the center of the free surface. These results suggest that the sloshing dynamical responses of the free surface show an increasing uncertainty sensitivity as one moves further from the shell wall. The influence of uncertainties on the indirect coupling mechanism (detailed in Section 2.5) is then analyzed. Figures 10 and 11 display the frequency responses at nodes $\mathbf{x}_1^h$ and $\mathbf{x}_2^h$ in the frequency band $[0\,,\,130]\,Hz$. It can be seen that the sloshing resonances, excited by the indirect transfer of energy from the structural nonlinearities, are robust to structural uncertainties.

5. Statistical inverse problem for uncertainty quantification

This section is devoted to the statistical inverse problem introduced for identifying the hyperparameter δ. For illustrating such an identification methodology, a dataset of simulated experiments in constructed, as explained in Section 1. It consists in generating a dataset of simulated experiments using the SROM for which the hyperparameter of the stochastic model, denoted by δ^{exp}, is given. The validation of the statistical inverse problem consists in comparing the identified optimal value δ^{opt} with δ^{exp}. The statistical inverse problem is formulated as an optimization problem for which the cost function corresponds to a least-square formulation.

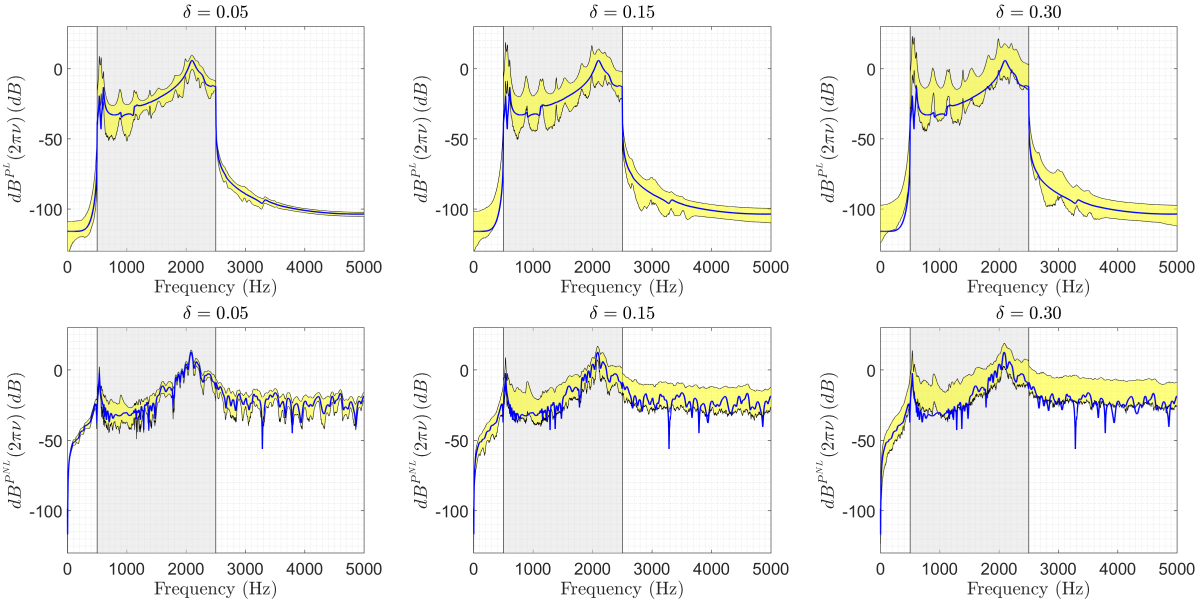

Figure 7: Nominal dynamical responses and confidence regions at 95% of the linear (top figures) and nonlinear (bottom figures) acoustic pressure at the observation point $\mathbf{x}^p$ for $\delta = 0.05$ (left), for $\delta = 0.15$ (middle), and for $\delta = 0.30$ (right).

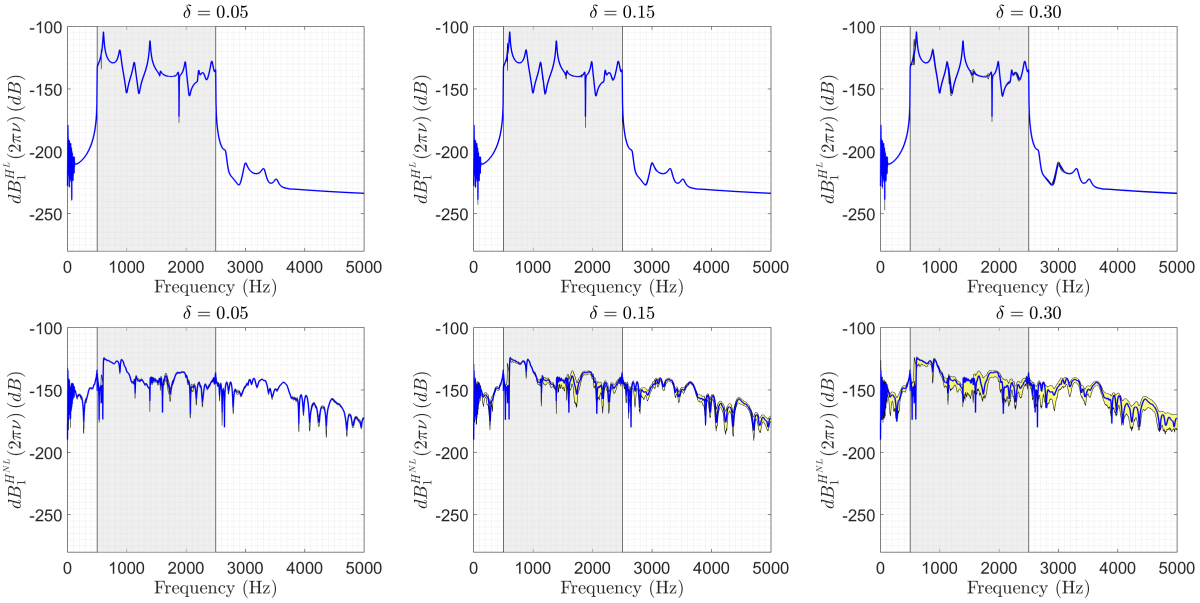

Figure 8: Nominal dynamical responses and confidence regions at 95% of the linear (top figures) and nonlinear (bottom figures) free-surface elevation at the observation point $\mathbf{x}_1^h$ for $\delta = 0.05$ (left), for $\delta = 0.15$ (middle), and for $\delta = 0.30$ (right).

5.1. Generating the dataset of simulated experiments

As explained above, this target dataset is constituted of N_r^{exp} independent realizations computed using the SROM. The simulated frequency response functions are observed at *experimental* points defined in Figure 12. These observation points have been chosen in order to potentially reproduce experimental setup conditions. For this reason, the inverse identification of hyperparameter δ does not take into account experimental data on the free-surface. There are $n_p^{\text{obs}} = 30$ observations for the acoustic pressure (blue dots

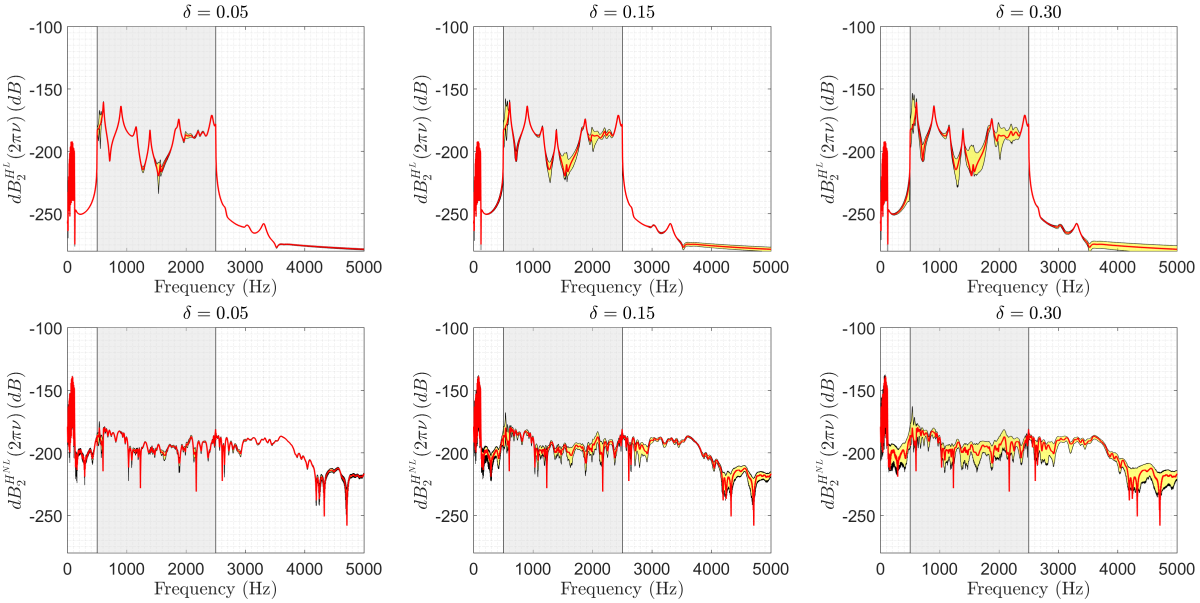

Figure 9: Nominal dynamical responses and confidence regions at 95% of the linear (top figures) and nonlinear (bottom figures) free-surface elevation at the observation point $\mathbf{x}_2^h$ for $\delta = 0.05$ (left), for $\delta = 0.15$ (middle), and for $\delta = 0.30$ (right).

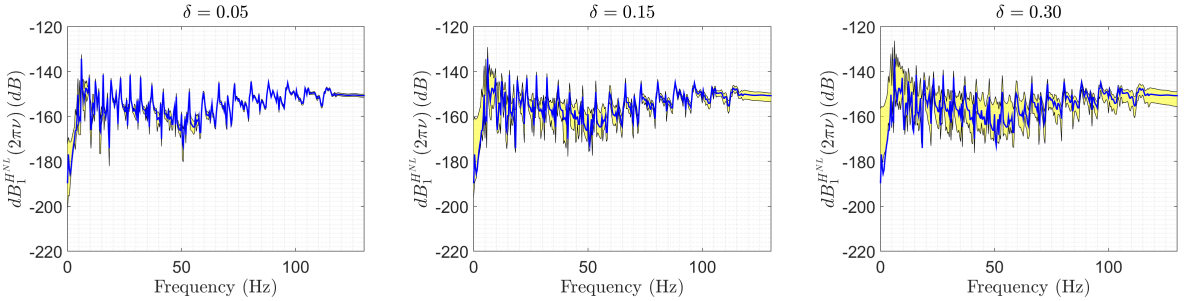

Figure 10: Nominal dynamical responses and confidence regions at 95% of the linear (top figures) and nonlinear (bottom figures) free-surface elevation at the observation point $\mathbf{x}_1^h$ for $\delta = 0.05$ (left), for $\delta = 0.15$ (middle), and for $\delta = 0.30$ (right), displayed over $[0, 130]\, Hz$.

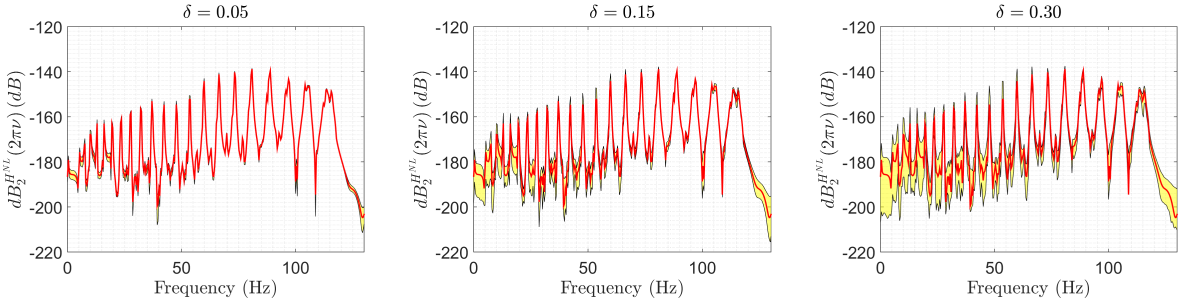

Figure 11: Nominal dynamical responses and confidence regions at 95% of the linear (top figures) and nonlinear (bottom figures) free-surface elevation at the observation point $\mathbf{x}_2^h$ for $\delta = 0.05$ (left), for $\delta = 0.15$ (middle), and for $\delta = 0.30$ (right), displayed over $[0, 130]\, Hz$.

in Figure 12) and $n_u^{\text{obs}} = 30$ observations for the structural displacement (red dots in Figure 12). For the

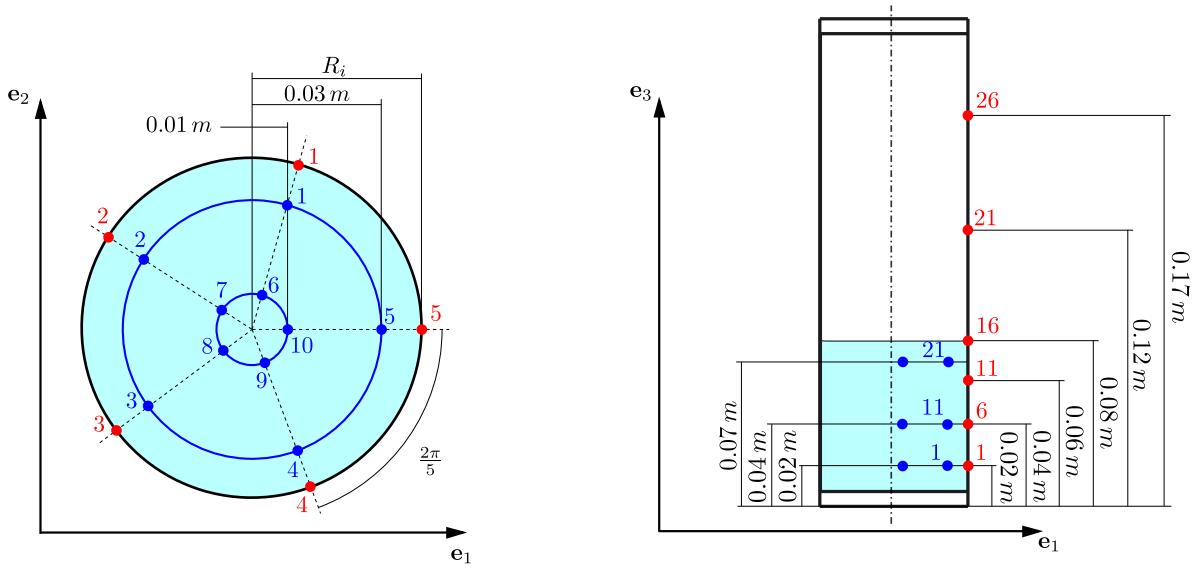

Figure 12: Position of the observation points for the stochastic problem.

structural displacement of the elastic structure, the corresponding quantities of interest are defined by

$$dB_i^{U,\exp}(2\pi\nu) = 20\log_{10}\left(\|\widehat{\mathbf{U}}^{\mathrm{NL},\exp}_{\mathbf{x}_i^u}(2\pi\nu)\|_{\mathbb{C}^3}\right)\,, \tag{30}$$

at the 30 observation points $\mathbf{x}_i^u$, $i = 1,\ldots,n_u^{\mathrm{obs}}$. The quantities of interest related to the acoustic liquid are defined by

$$dB_i^{P,\exp}(2\pi\nu) = 20\log_{10}(\,|\widehat{\mathbf{P}}^{\mathrm{NL},\exp}_{\mathbf{x}_i^p}(2\pi\nu)|\,)\,, \tag{31}$$

for the 30 observation points $\mathbf{x}_i^p$, $i = 1,\ldots,n_p^{\mathrm{obs}}$, in the internal liquid.

5.2. Definition of the cost function

For estimating the optimal value of hyperparameter δ, the cost function is defined in the framework of the least-square method. This method consists in calculating the optimal value δ^{opt} of δ, such that

$$\delta^{\mathrm{opt}} = \arg\min \mathscr{J}(\delta)\,, \tag{32}$$

in which $\mathscr{J}(\delta)$ is written as

$$\mathscr{J}(\delta) = \mathscr{J}_1(\delta) + \mathscr{J}_2(\delta)\,, \tag{33}$$

in which $\mathscr{J}_1(\delta)$ is related to the mean value and $\mathscr{J}_2(\delta)$ to the standard deviation of the random responses. The cost function $\mathscr{J}_1(\delta)$ is expressed as the sum of a cost function for the structure and a cost function for the liquid as

$$\mathscr{J}_1(\delta) = \mathscr{J}_1^U(\delta) + \mathscr{J}_1^P(\delta)\,, \tag{34}$$

in which, for $X \in \{U, P\}$,

$$\mathscr{J}_1^X(\delta) = \frac{\displaystyle\int_{\mathbb{B}_a} \sum_{k=1}^{n_{\mathrm{obs}}^X} \Big(E\{\,dB_k^X(2\pi\nu;\delta)\,\} - E\{\,dB_k^{X,\exp}(2\pi\nu)\,\}\Big)^2 d\nu}{\displaystyle\int_{\mathbb{B}_a} \sum_{k=1}^{n_{\mathrm{obs}}^X} \Big(E\{\,dB_k^{X,\exp}(2\pi\nu)\,\}\Big)^2 d\nu}\,. \tag{35}$$

Similarly, the cost function $\mathscr{J}_2(\delta)$ is expressed as the sum of a cost function for the structure and a cost function for the liquid as

$$\mathscr{J}_2(\delta) = \mathscr{J}_2^U(\delta) + \mathscr{J}_2^P(\delta)\,, \tag{36}$$

in which, for $X \in \{U, P\}$,

$$\mathscr{J}_2^X(\delta) = \frac{\displaystyle\int_{\mathbb{B}_a} \left(\,\Delta^X(2\pi\nu,\delta) - \Delta^{X,\exp}(2\pi\nu)\,\right)^2 d\omega}{\displaystyle\int_{\mathbb{B}_a} \Delta^{X,\exp}(2\pi\nu)\, d\omega}\,. \tag{37}$$

In Eq. (37), the quantity $\Delta^X(2\pi\nu,\delta)$ is written as

$$\Delta^X(2\pi\nu,\delta) = \left(\frac{E\left\{\displaystyle\sum_{k=1}^{n_{\rm obs}^X} dB_k^X(2\pi\nu,\delta)^2\right\} - \displaystyle\sum_{k=1}^{n_{\rm obs}^X} \left\{E(dB_k^X(2\pi\nu,\delta))\right\}^2}{\displaystyle\sum_{k=1}^{n_{\rm obs}^X} \left\{E(dB_k^X(2\pi\nu,\delta))\right\}^2} \right)^{\frac{1}{2}}\,, \tag{38}$$

and the quantity $\Delta^{X,\exp}(2\pi\nu)$ is defined by Eq. (38) in which dB^X is replaced by $dB^{X,\exp}$.

5.3. Identification of the optimal hyperparameter δ^{opt}

A numerical illustration is presented hereinafter in which the optimal parameter $\delta^{\rm opt}$ is evaluated using the inverse problem methodology, and is compared to the dispersion parameter $\delta^{\rm exp} = 0.3$ used for generating the dataset of $N_r^{\rm exp}$ simulated experiments. Figure 13 displays the graphs of 6 cost functions $\mathscr{J}(\delta)$ estimated for 6 different values $N_r^{\rm exp} \in \{5, 10, 20, 60, 120, 200\}$. In Figure 13, it can be seen that the estimated optimal hyperparameter $\delta^{\rm opt}$ converges to $\delta^{\rm exp} = 0.3$ with respect to $N_r^{\rm exp}$.

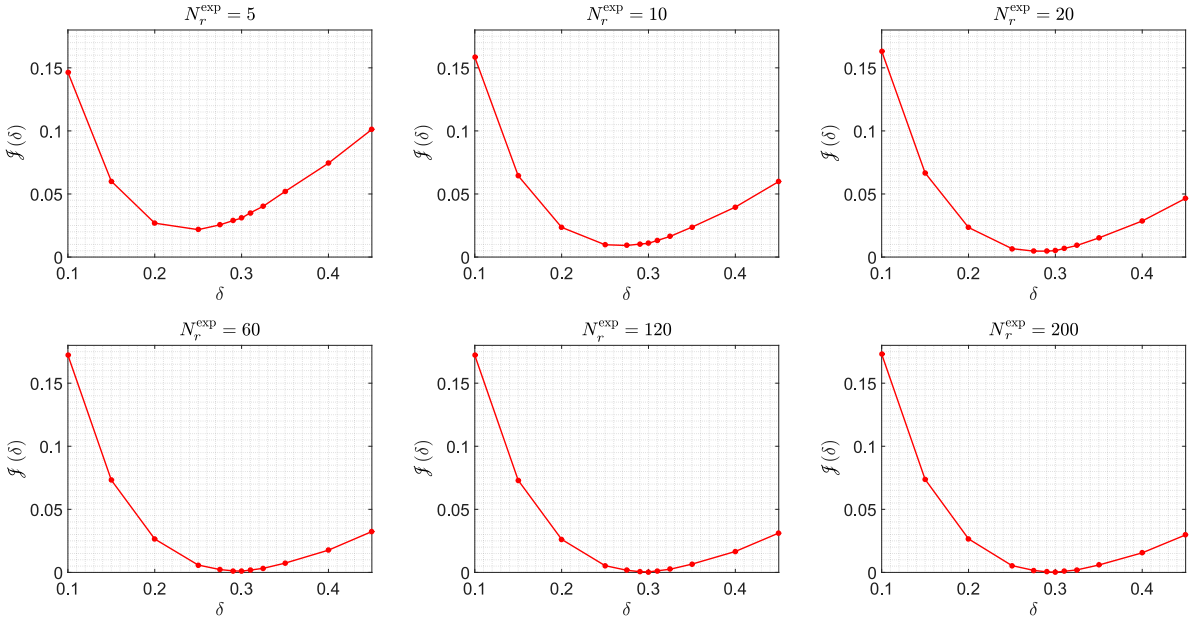

Figure 13: Graphs of $\delta \mapsto \mathscr{J}(\delta)$ displaying the cost function $\mathscr{J}(\delta)$ with respect to the hyperparameter δ for 6 values of $N_r^{\rm exp} \in \{5, 10, 20, 60, 120, 200\}$.

6. Conclusions and discussions

In this paper, we have presented an uncertainty quantification analysis of the fluid-structure system experimentally studied in the sixties by Abramson, Kana, and Lindholm. The dynamical behavior of this nonlinear complex fluid-structure system has been analyzed in a previous work. Nevertheless, due to the unexpected experimental sloshing phenomenon, which appears at very low-frequency and which has been explained by a very small amount of energy that is transferred from the structure to the free surface via the acoustic liquid, it was necessary to analyze the sensitivity of this phenomenon with respect to structural uncertainties.

The sensitivity analysis with respect to structural uncertainties has been carried out by varying the uncertainty levels controlled by the hyperparameter of the probabilistic model. The results show a significant, if not a great, sensitivity of the displacement of the structure, of the acoustic pressure in the liquid, and of the free-surface elevation to uncertainties in both linear and geometrically nonlinear simulations. Note that the sloshing dynamical responses of the free surface show an increasing uncertainty sensitivity as one moves further from the shell wall. Indeed, the points on the free surface, which are the most distant from the structure, show a higher level of sensitivity to uncertainty than those on the triple line. However, a robustness (with respect to structural uncertainties) of the very low frequency sloshing resonances has been noticed. Finally, the feasability has been demonstrated for solving the inverse statistical problem concerning the identification of the hyperparameter of the stochastic model of structural uncertainties. Consequently if experiments were available for similar complex fluid-structure systems, such an approach could be reused.

Acknowledgements

This work has partially been supported by the DGA (Direction Générale de l'Armement) in France.

References

Abramson, H.N., Kana, D.D., Lindholm, U.S., 1966. An experimental study of liquid instability in a vibrating elastic tank. Journal of Spacecraft and Rockets 3, 1183–1188.

Akkaoui, Q., Capiez-Lernout, E., Soize, C., Ohayon, R., 2018. Solving generalized eigenvalue problems for large scale fluid-structure computational models with mid-power computers. Computers & Structures 205, 45–54.

Akkaoui, Q., Capiez-Lernout, E., Soize, C., Ohayon, R., 2019. Revisiting the experiment of a free-surface resonance of a liquid in a vibration tank using a nonlinear fluid–structure computational model. Journal of Fluids and Structures 85, 149–164.

Amabili, M., 2018. Nonlinear Mechanics of Shells and Plates: Composite, Soft and Biological Materials. Cambridge University Press, Cambridge.

Amabili, M., Paıdoussis, M.P., 2003. Review of studies on geometrically nonlinear vibrations and dynamics of circular cylindrical shells and panels, with and without fluid-structure interaction. Applied Mechanics Reviews 56, 349–381.

Amabili, M., Sarkar, A., Paıdoussis, M., 2003. Reduced-order models for nonlinear vibrations of cylindrical shells via the proper orthogonal decomposition method. Journal of Fluids and Structures 18, 227–250.

Amabili, M., Touzé, C., 2007. Reduced-order models for nonlinear vibrations of fluid-filled circular cylindrical shells: comparison of POD and asymptotic nonlinear normal modes methods. Journal of Fluids and Structures 23, 885–903.

Ballarin, F., Rozza, G., 2016. POD–galerkin monolithic reduced order models for parametrized fluid-structure interaction problems. International Journal for Numerical Methods in Fluids 82, 1010–1034.

Brakke, K.A., 1992. The surface evolver. Experimental mathematics 1, 141–165.

Capiez-Lernout, E., Soize, C., 2017. An improvement of the uncertainty quantification in computational structural dynamics with nonlinear geometrical effects. International Journal for Uncertainty Quantification 7, 83–98.

Capiez-Lernout, E., Soize, C., Mignolet, M., 2012. Computational stochastic statics of an uncertain curved structure with geometrical nonlinearity in three-dimensional elasticity. Computational Mechanics 49, 87–97.

Carra, S., Amabili, M., Garziera, R., 2013. Experimental study of large amplitude vibrations of a thin plate in contact with sloshing liquids. Journal of Fluids and Structures 42, 88–111.

Chiba, M., 1992. Nonlinear hydroelastic vibration of a cylindrical tank with an elastic bottom, containing liquid. part I: Experiment. Journal of Fluids and Structures 6, 181–206.

Ghanem, R., Higdon, D., Owhadi, H., 2017. Handbook of Uncertainty Quantification. volume 6. Springer, New York.

Ghanem, R.G., Spanos, P.D., 1991. Stochastic Finite Elements: a Spectral Approach. Springer-Verlag, Berlin, Heidelberg.

Lindholm, U.S., Kana, D.D., Abramson, H.N., 1962. Breathing vibrations of a circular cylindrical shell with an internal liquid. Journal of the Aerospace Sciences 29, 1052–1059.

Mignolet, M.P., Przekop, A., Rizzi, S.A., Spottswood, S.M., 2013. A review of indirect/non-intrusive reduced order modeling of nonlinear geometric structures. Journal of Sound and Vibration 332, 2437–2460.
Mignolet, M.P., Soize, C., 2008. Stochastic reduced order models for uncertain geometrically nonlinear dynamical systems. Computer Methods in Applied Mechanics and Engineering 197, 3951–3963.
Morand, H.J., Ohayon, R., 1995. Fluid Structure Interaction. John Wiley & Sons, New York, (French edition, Masson, Paris, 1992).
Ohayon, R., Soize, C., 2016. Nonlinear model reduction for computational vibration analysis of structures with weak geometrical nonlinearity coupled with linear acoustic liquids in the presence of linear sloshing and capillarity. Computers & Fluids 141, 82 – 89.
Schueller, G., 2007. On the treatment of uncertainties in structural mechanics and analysis. Computers & structures 85, 235–243.
Soize, C., 2000. A nonparametric model of random uncertainties for reduced matrix models in structural dynamics. Probabilistic Engineering Mechanics 15, 277–294.
Soize, C., 2017. Uncertainty Quantification: An Accelerated Course with Advanced Applications in Computational Engineering. Springer, New York.

Appendix A. Brief recall on the nonparametric probabilistic approach of uncertainties

In the nonparametric probabilistic approach of uncertainties, the uncertainties are taken in account by substituting deterministic matrices of the ROM by random matrices yielding a stochastic reduced-order model (SROM). The probability distributions and the generators of independent realizations of random matrices that are used are constructed using the ensembles of random matrices introduced in (Soize, 2000, 2017).

(i) - Ensemble SG_0^+ *and its generator*

An element of ensemble SG_0^+ is the random matrix $[\mathbf{G}_0]$ with values in $\mathbb{M}_m^+$ for which its probability density function is defined by

$$p_{[\mathbf{G}_0]}([G]) = \mathbb{1}_{\mathbb{M}_m^+}([G])\ c_0(\det[G])^{c_1} \exp\{-c_2\,\mathrm{Tr}([G])\}\,, \tag{A.1}$$

in which c_0 the positive constant of normalization, where $c_1 = (m+1)(1-\delta^2)/(2\delta^2)$, and where $c_2 = (m+1)/(2\delta^2)$ depend on dimension m and on a hyperparameter $\delta \in [0\,,\,\delta_{\max}[$. Such a random matrix $[\mathbf{G}_0]$ admits the following algebraic representation that can be used as a generator of independent realizations,

$$[\mathbf{G}_0] = [\mathbf{L}]^T\,[\mathbf{L}]\,, \tag{A.2}$$

in which $[\mathbf{L}]$ is an upper triangular $(m \times m)$ random matrix such that:

- random variables $\{[\mathbf{L}]_{jj'}, j \leq j'\}$ are independent.
- For $j < j'$, the real-valued random variable $[\mathbf{L}]_{jj'}$ is written as $[\mathbf{L}]_{jj'} = \sigma_m\, A_{jj'}$ in which $\sigma_m = \delta(m+1)^{-1/2}$ and where $A_{jj'}$ is a real-valued Gaussian random variable with zero mean and variance equal to 1.
- For $j = j'$, the positive-valued random variable $[\mathbf{L}]_{jj}$ is written as $[\mathbf{L}]_{jj} = \sigma_m\sqrt{2B_j}$, in which B_j is a positive-valued Gamma random variable with probability density function $\Gamma(a_j, 1)$, in which $a_j = \frac{m+1}{2\delta^2} + \frac{1-j}{2}$.

The positive parameter δ is the hyperparameter of the probability distribution of random matrix $[\mathbf{G}_0]$, which is such that

$$\delta = \left\{ \frac{1}{m} E\{\| [\mathbf{G}_0] - [I_m] \|_F^2\} \right\}^{\frac{1}{2}}\,, \tag{A.3}$$

and which allows the dispersion of matrix $[\mathbf{G}_0]$ to be controlled. The hyperparameter δ must be such that $0 \leq \delta \leq \delta_{\max} = (m+1)^{\frac{1}{2}}(m+5)^{-\frac{1}{2}}$.

(ii) - Ensemble SE_0^+ *of random matrices*

Let $[A]$ be a deterministic positive-definite matrix representing the given mean value. SE_0^+ is the ensemble of positive-definite random matrices such that any positive-definite random matrix $[\mathbf{A}_0]$ in SE_0^+ satisfies

$$E\{[\mathbf{A}_0]\} = [A]\ ,\ E\{\mathrm{Log}(\det([\mathbf{A}_0]))\} = \nu_{[\mathbf{A}_0]}\ ,\ \nu_{[\mathbf{A}_0]} < +\infty\ . \tag{A.4}$$

Random matrix $[\mathbf{A}]$ can then be written as

$$[\mathbf{A}_0] = [L_A]^T\,[\mathbf{G}_0]\,[L_A]\ ,\ [\mathbf{G}_0] \in \mathrm{SG}_0^+\ , \tag{A.5}$$

in which $[A] = [L_A]^T\,[L_A]$ is the Cholesky factorization of $[A]$.

(iii) - Ensemble $\mathrm{SE}_\varepsilon^+$ *of random matrices*

For fixed $\varepsilon > 0$, any random matrix $[\mathbf{A}]$ in $\mathrm{SE}_\varepsilon^+$ is a random matrix with values in $\mathbb{M}_m^+$, which is written as

$$[\mathbf{A}] - [A_\ell] = \frac{1}{1+\varepsilon}[\mathbf{A}_0] > 0 \text{ a.s. with } [\mathbf{A}_0] \in \mathrm{SE}_0^+\ , \tag{A.6}$$

where $[A_\ell] \in \mathbb{M}_m^+$ is the positive-definite lower bound that is presently defined by

$$[A_\ell] = c_\varepsilon\,[A] \text{ with } c_\varepsilon = \frac{\varepsilon}{1+\varepsilon}\ . \tag{A.7}$$

Consequently, $E\{[\mathbf{A}]\} = [A]$. If $\varepsilon = 0$, then ensemble $\mathrm{SE}_\varepsilon^+$ coincides with SE_0^+. For $\varepsilon > 0$, this ensemble allows for introducing a positive-definite lower bound $[A_\ell]$ that is arbitrarily constructed for the case where it is known that a lower bound exists but for which there are no available information for identifying it. That is the case considered here and ε will be chosen as 10^{-6} in the application. The generator of independent realization of $[\mathbf{A}]$ in $\mathrm{SE}_\varepsilon^+$ is then deduced from the one presented for SG_0^+.